Original article

MOLECULAR METABOLISM

Super-enhancer-driven LncRNA *PPARα–seRNA* exacerbates glucolipid metabolism and diabetic cardiomyopathy via recruiting KDM4B

Xiaozhu Ma[1,2,4], Shuai Mei[1,2,4], Qidamugai Wuyun[1,2], Li Zhou[1,2], Ziyang Cai[1,2], Hu Ding[1,2,3,], Jiangtao Yan[1,2,*]**

ABSTRACT

Objective: Aberrant glucolipid metabolism in the heart is a characteristic factor in diabetic cardiomyopathy (DbCM). Super-enhancers-driven noncoding RNAs (seRNAs) are emerging as powerful regulators in the progression of cardiac diseases. However, the functions of seRNAs in DbCM have not been fully elucidated.

Methods: Super enhancers and their associated seRNAs were screened and identified by H3K27ac ChIP-seq data in the Encyclopedia of DNA Elements (ENCODE) dataset. A dual-luciferase reporter assay was performed to analyze the function of super-enhancers on the transcription of peroxisome proliferator-activated receptor α-related seRNA (*PPARα-seRNA*). A DbCM mouse model was established using db/db leptin receptor-deficient mice. Adeno-associated virus serotype 9-seRNA (AAV9-seRNA) was injected via the tail vein to evaluate the role of seRNA in DbCM. The underlying mechanism was explored through RNA pull-down, RNA and chromatin immunoprecipitation, and chromatin isolation by RNA purification.

Results: *PPARα-seRNA* was regulated by super-enhancers and its levels were increased in response to high glucose and palmitic acid stimulation in cardiomyocytes. Functionally, *PPARα-seRNA* overexpression aggravated lipid deposition, reduced glucose uptake, and repressed energy production. In contrast, *PPARα-seRNA* knockdown ameliorated metabolic disorder *in vitro*. *In vivo*, overexpression of *PPARα-seRNA* exacerbated cardiac metabolic disorder and deteriorated cardiac dysfunction, myocardial fibrosis, and hypertrophy in DbCM. Mechanistically, *PPARα-seRNA* bound to the histone demethylase KDM4B (Lysine-specific demethylase 4B) and decreased H3K9me3 levels in the promoter region of PPARα, ultimately enhancing its transcription.

Conclusions: Our study revealed the pivotal function of a super-enhancer-driven long noncoding RNA (lncRNA), *PPARα-seRNA*, in the deterioration of cardiac function and the exacerbation of metabolic abnormalities in diabetic cardiomyopathy, which recruited KDM4B to the promoter region of PPARα and repression of its transcription. This suggests a promising therapeutic strategy for the treatment of DbCM.

Keywords Diabetic cardiomyopathy; Glucolipid metabolism; SeRNA; PPARα; KDM4B

1. INTRODUCTION

Diabetic cardiomyopathy (DbCM), a typical clinical entity caused by metabolic disorders, leads to heart failure with preserved ejection fraction (HFpEF) or with reduced ejection fraction (HFrEF), even in the absence of other cardiac risk factors such as coronary heart disease, hypertension, or valvular disease [1,2]. Glucolipid metabolism disorder, as an initial and primary factor of DbCM, elicits a shift of the main metabolic substrate from glucose to fatty acids, and results in decreased energy utilization. This predominance of fatty acids in the heart leads to sugar and lipid toxicity, which triggers serious inflammation, oxidative stress, and cascade reactions [3–5]. Therefore, elucidating the underlying mechanisms of glucolipid metabolism disorders is imperative for establishing efficacious therapeutic strategies for DbCM.

Super enhancers (SEs) are cis-acting genomic DNA elements enriched with large clusters of enhancers. They are occupied with abnormally high levels of master transcription factors, active histone marks

[1]Division of Cardiology, Departments of Internal Medicine, Tongji Hospital, Tongji Medical College, Huazhong University of Science and Technology, Wuhan, China [2]Hubei Key Laboratory of Genetics and Molecular Mechanisms of Cardiological Disorders, Wuhan, China [3]Key Laboratory of Vascular Aging, Ministry of Education, Tongji Hospital of Tongji Medical College, Huazhong University of Science and Technology, China

[4] Xiaozhu Ma and Shuai Mei contributed equally to this work.

*Corresponding author. Division of Cardiology, Departments of Internal Medicine, Tongji Hospital, Tongji Medical College, Huazhong University of Science and Technology, 1095# Jiefang Ave, Wuhan 430030, China. Tel./fax: +86 27 8366 3280. E-mail: jtyan@tjh.tjmu.edu.cn (J. Yan).

**Corresponding author. Division of Cardiology, Departments of Internal Medicine, Tongji Hospital, Tongji Medical College, Huazhong University of Science and Technology, Wuhan, China. E-mail: huding@tjh.tjmu.edu.cn (H. Ding).

Received April 7, 2024 • Revision received June 17, 2024 • Accepted June 24, 2024 • Available online 29 June 2024

https://doi.org/10.1016/j.molmet.2024.101978

(H3K27ac), and the transcription regulator factors MED1, BRD4, Pol II and p300, among others [6]. Super enhancers serve as key nodes regulating disease progression, and they are frequently identified near critical genes or ncRNAs involved in modulating cell biology [7–9]. SEs are transcribed into noncoding RNAs (ncRNAs), termed seRNAs, which comprise long noncoding RNAs (lncRNA), circular RNAs (circRNA) and microRNAs (miRNA). They have been reported to play critical roles in cardiac pathophysiology, broadening our understanding of the function of noncoding RNAs in heart tissue [10–12]. The seRNA *Wisper* increases in cardiac fibroblasts after myocardial infarction and participates in cardiac fibrosis and remodeling processes [13]. Super enhancer-regulated circNfix plays an important role in cardiac regeneration after myocardial infarction [14]. However, reports on seRNAs in the pathophysiological settings of glucolipid metabolism disorder and DbCM are scarce.

In this study, we identified a novel super enhancer-driven ncRNA, known as *PPARα-seRNA*, involved in glucolipid metabolism disorder during DbCM, and further revealed its function and underlying mechanism of action. Our results suggest that *PPARα-seRNA*, as a key epigenetic regulator of glucolipid metabolism disorder, may be particularly attractive as a therapeutic target for the treatment of diabetic cardiomyopathy.

2. MATERIALS AND METHODS

2.1. Construction of diabetic cardiomyopathy mouse model

Male db/db and db/wt mice were purchased from GemPharmatech Co., Ltd. (Jiangsu, China) and fed with a normal diet to 24 weeks of age in an SPF-level barrier facility. Then, the mice were euthanized by intraperitoneal injection of xylazine (5 mg/kg) and ketamine (80 mg/kg) for further analysis of the cardiac tissue. All animal procedures were carried out with the approval of the Experimental Animal Research Committee of Tongji Medical College, Huazhong University of Science and Technology, and adhered to the rules of the Care and Use of Laboratory Animals of the National Institutes of Health ([2021] IACUC number: 3279).

2.2. Cell culture and transfection

AC16 human cardiomyocyte-like cells, murine HL-1 cardiomyocyte-like cells, and HEK293T cell lines from ATCC (Manassas, VA, USA) were maintained in Dulbecco's modified Eagle's medium (DMEM, 5% glucose) supplemented with 10% Fetal Bovine Serum (FBS) and 1% of penicillin/streptomycin mixture, and cultured at 37 °C in a humidified atmosphere of 5% CO2. SiRNAs targeting KDM4B or PPARα were designed and constructed by Aoke Biocompany (Wuhan, China). Transfections were performed using Lipofectamine 2000 (Life Technologies, Carlsbad, CA, USA) for 48 h when the cell density reached 50–60%. The cells were subsequently harvested for qRT-PCR and western blot analysis. The sequences of the siRNA used in the experiments are listed in Table S4.

2.3. Quantitative real-time polymerase chain reaction (qRT-PCR)

Total RNA was extracted by Trizol reagent (Vazyme, Nanjing, China) according tothe manufacturer's procedures. Reverse transcription was implemented by HiScript II 1st Strand cDNA Synthesis Kit (Vazyme, Nanjing, China), and cDNA was obtained. Quantitative real-time quantitative polymerase chain reaction was performed by SYBR Green I assay on a 7900 HT Fast Real-Time PCR machine (Applied Biosystems, Foster City, CA). Gene expression was normalized to α-tubulin and quantified by the 2- ΔΔCt algorithm. The sequence of the primers used in the experiments is listed in Table S1.

2.4. Protein extraction and western blot

Total proteins were isolated after lysis of the cultures in IP lysis buffer (Beyotime, Shanghai, China), followed by centrifugation at 12,000 rpm for 15 min at 4 °C. The proteins were separated in acrylamide gels with appropriate voltage and current and transferred to PVDF membranes. The membranes were incubated overnight with primary antibodies (1:1000 ratio). After washing three times with TBST (TBS and 0.1% Tween-20), the membranes were incubated with a secondary antibody for 1 h, and the proteins were quantified using a chemiluminescence imager. The antibodies used in this study are listed in Table S6.

2.5. Isolation of the nuclear and cytoplasmic fractions

Cellular fractions were separated using a Nucl-Cyto-Mem Preparation Kit (Cat# 9038; Cell Signalling Technology, Danvers, MA, USA) according to the manufacturer's protocol. The level of *PPARα-seRNA*, U6 and GAPDH were measured by qRT-PCR. Western blot was used to analyze Lamin B1 and GAPDH for quality control.

2.6. RNA fluorescent *in situ* hybridization (FISH)

The location of *PPARα-seRNA* in AC16 cells was evaluated by fluorescent *in situ* hybridization. Firstly, cells were fixed in 4% paraformaldehyde for 30 min after being washed with PBS twice. Then, 0.5% Triton-100 was used to permeabilize them. The cells were blocked in prehybridization solution at 55 °C for 20 min and then incubated with a hybridization system (10pmoL DIG-labeled probe) at 55 °C without light for 1 h. Then, the cells were washed sequentially with three hybrid lotions at 60 °C and counterstained with DAPI dye (1:1000 in PBS). Finally, the signal from the probes were amplified using the TSA system (G1236, Servicebio, Wuhan, China) and measured with an inverted fluorescence microscope (TE 2000, Nikon, Japan) with Zen blue system. The sequence of the DIG-labeled probes used in the experiment is shown in Table S3.

2.7. CRISPR/dCAS9 and sgRNA construct design

To modulate enhancer activities, we designed single guide RNAs (sgRNAs) and assessed their specificity using a cloud-based platform for biotechnology research and development, Benchling. Subsequently, the sgRNAs were integrated into either the dCAS9-KRAB or dCAS9-p300 lentiviral vectors to facilitate the repression or activation of enhancers, respectively. The sgRNA sequence is listed in Table S2.

2.8. RNA pull-down assay

A PCR assay was performed with a specific primer containing the T7 promoter amplified PPARa-seRNA double strand. PPARa-seRNA sense and antisense strands tagged with biotin were obtained via reverse transcription, as previously described [15]. The RNA pull-down assay was performed using a Pierce Magnetic RNA-Protein Pull-Down Kit (Thermo Fisher Scientific, USA). The streptavidin magnetic beads were washed twice with 20 mM Tris (pH 7.5) and mixed with 1 × RNA Capture Buffer and PPARa-seRNA for 1 h at room temperature. The cells were collected and added to RNA-magnetic complexes for further incubation with an RNA-protein binding reaction system. Then, the samples were washed with IP lysate. Target proteins were identified by mass spectrometry analysis or western blot. The primer sequence targeting *PPARα-seRNA* is listed in Table S5. The proteins detected by mass spectrometry are listed in Table S7.

2.9. RNA immunoprecipitation assay

The RNA immunoprecipitation assay was performed using the Magan RIPTMRNA—Binding Protein Immunoprecipitation Kit (Millipore, USA)

based on the manufacturer's instructions. Anti-KDM4B or Anti-IgG antibodies (Abclonal, Wuhan, China) were incubated with protein A/G Magnetic Beads (MCE, Shanghai, China) at room temperature for 1 h. Then, lysed cell extracts were added to the bead-antibody complexes with the RIP IP buffer system (0.5M EDTA, RNase inhibitor, and wash buffer). The enriched RNAs were eluted and extracted using the Trizol reagent.

2.10. Co-immunoprecipitation

Cells were harvested and collected, followed by the addition of lysis buffer and incubation on ice for 30 min to facilitate cell lysis. Then, the lysate was centrifuged at 12,000 rpm for 4 °C, and the supernatant was collected. Next, the supernatant was incubated with the primary antibody at room temperature with constant rotation for 2 h to form antibody—antigen complex. Subsequently, the antigen—antibody complexes were incubated with protein A/G magnetic beads at room temperature with rotation for 2 h. After that, the bound complexes were washed by wash buffer and eluted by loading buffer. The products were then used for mass spectrometry identification or Western blot. The proteins identified by mass spectrometry were listed in Table S8.

2.11. ChIP-PCR

The ChIP assay was carried out according to the manufacturer's instructions (Beyotime, Shanghai, China). Firstly, cells were incubated in 1% formaldehyde solution at 37 °C for 10 min and cross-linked in 10× glycine solution at room temperature. Secondly, the cells were washed in PBS containing 1 mM PMSF and centrifuged at 1000g at 4 °C. After discarding the supernatant, the cells were resuspended in SDS lysis buffer containing 1 mM PMSF. The samples were treated with ultrasonic waves (200 W) 10 times until the supernatant was clear. The cells were then incubated overnight with anti-KDM4B and anti-H3K9me3 antibodies (Abclonal) at 4 °C. The next day, the protein A/G Magnetic Beads (MCE, Shanghai, China) were added to the samples for 1 h and washed with four wash buffers. The extracted and purified DNA was quantified by qRT-PCR using pre-designed primers targeting the PPARα promoter region. The sequences of the primers used for this experiment is listed in Table S1.

2.12. Cardiac echocardiograph

Mice were anesthetized with 1.5%—2% isoflurane, and cardiac structure and function was detected using the Vevo 2100 echocardiography system (Vevo770, VisualSonics) with a 30 MHz central high-frequency scan head. The cardiac long and short axis were measured from M-mode images at the papillary muscle level. Cardiac parameters, including ejection fraction and fractional shortening, were analyzed using PVAN software (Millar Instruments, Inc., Houston, TX). Fractional shortening was calculated as (end left ventricle [LV] diastolic diameter − end LV systolic diameter) × 100%/end LV diastolic diameter. Ejection fraction was calculated as (end LV diastolic volume − end LV systolic volume) × 100%/end LV diastolic volume. The values were listed in Table S9.

2.13. Statistical analysis

Quantitative data derived from at least three experiments are presented as mean ± SEM and analyzed with GraphPad Prism (version 8.0, GraphPad Software, San Diego, CA, USA) and IBM SPSS Statistics 22.0 (IBM Corporation, USA). An unpaired two-tailed Student t-test was used to compare two groups, and one-way ANOVA with Tukey post hoc test to compare multiple groups. Repeated measures ANOVA was used to analyze the results of the glucose tolerance test (GTT) on db/db mice. A p-value <0.05 was considered statistically significant for all tests.

3. RESULTS

3.1. Identification of *PPARα-seRNA* participating in glucolipid metabolism disorder

Emerging evidence has proven that super-enhancers and SE-driven non-coding RNAs (seRNAs) play a crucial role in the progress of metabolic diseases. Given the core roles of liver, small intestine, pancreas and adipose in glucose and lipid metabolism, we speculated that those epigenetic agents profusely expressed in these metabolic organs may play a key role in glucolipid metabolic disorders, including diabetic cardiomyopathy. We identified critical seRNAs involved in metabolism disorder by analyzing H3K27ac ChIP-seq data of different metabolic tissues (liver, intestine, pancreas, and adipose) and heart from the Encyclopedia of DNA Elements (ENCODE; https://www.encodeproject.org) according to the Rank Ordering of Super-Enhancers (ROSE) algorithm (Figure 1A—B & Figure S1A-D). Finally, four SE-lncRNAs were identified in the five selected tissues (Figure 1C). JQ1, a BET inhibitor, has dramatic potential to decrease the read of BRD4 to H3K27ac, and then is often used to identify super enhancers and their related genes [12,16]. Three lncRNAs were down-regulated in response to stimulation with JQ1 (Figure 1D). Further analysis indicated that LINC00899 had the highest expression, and the most significant upregulation in response to high glucose and palmitic acid compared with the other three seRNAs (Figure 1E). Therefore, we selected LINC00899 for further study and named it PPARα adjacent super-enhancer-regulated RNA (*PPARα-seRNA*) based on its position in the genome and its function. In order to characterize the role of *PPARα-seRNA* in metabolism regulation, we recorded changes of *PPARα-seRNA* levels following either inhibition or activations of AMP-activated protein kinase (AMPK), a key regulator of metabolism and mitochondrial homeostasis [17]. *PPARα-seRNA* levels were upregulated in response to AMPK inhibition and downregulated when AMPK was activated (Figure S2A).

The gene coding for *PPARα-seRNA* is located on chromosome 22 and consists of 4 exons and 3 introns (chr22:46,041,009-46,044,853; Figure 1F). *PPARα-seRNA* is more abundant in cardiomyocytes compared to cardiac fibroblasts and endothelial cells (Figure 1G), and present both in the cardiomyocyte nucleus and cytoplasm (Figure 1H—I). Furthermore, RNA sequencing data from the Genotype-Tissue Expression (GTEX) database indicated that *PPARα-seRNA* is widely distributed in human tissues and organs (Figure S2B). The human ortholog of *PPARα-seRNA* exhibits a nucleotide identity of 45.6% with its mouse counterpart *(lncPPARa)*. *lncPPARa* was upregulated in response to high glucose and palmitic acid and downregulated in response to JQ1 stimulation, in agreement with what has been observed in the case of *PPARα-seRNA* (Figure S3A-E). Bioinformatics tools, the Coding Potential Assessment Tool, and ORFinder were employed to determine the coding potential of the *PPARα-seRNA* sequence, and the ability to generate a peptide via translation was confirmed by western blot and immunoprecipitation assays (Figure S4A-E).

To further evaluate whether *PPARα-seRNA* was regulated by super enhancers in heart tissue, we analyzed the multiple ChIP-seq data of histone modifications from ENCODE. As expected, activated histone modification peaks, such as H3K27ac, H3K4me1 and H3K4me3, were present upstream of the *PPARα-seRNA* gene in the heart as well as in other four metabolic tissues (Figure 1I and Figure S1E). In contrast, the peaks corresponding to an inhibitory histone modification marker (H3K27me3) were not obvious. According to the condition of activated histone modifications of the super-enhancer, we subdivided it into four activating enhancers, and their sequences were inserted into

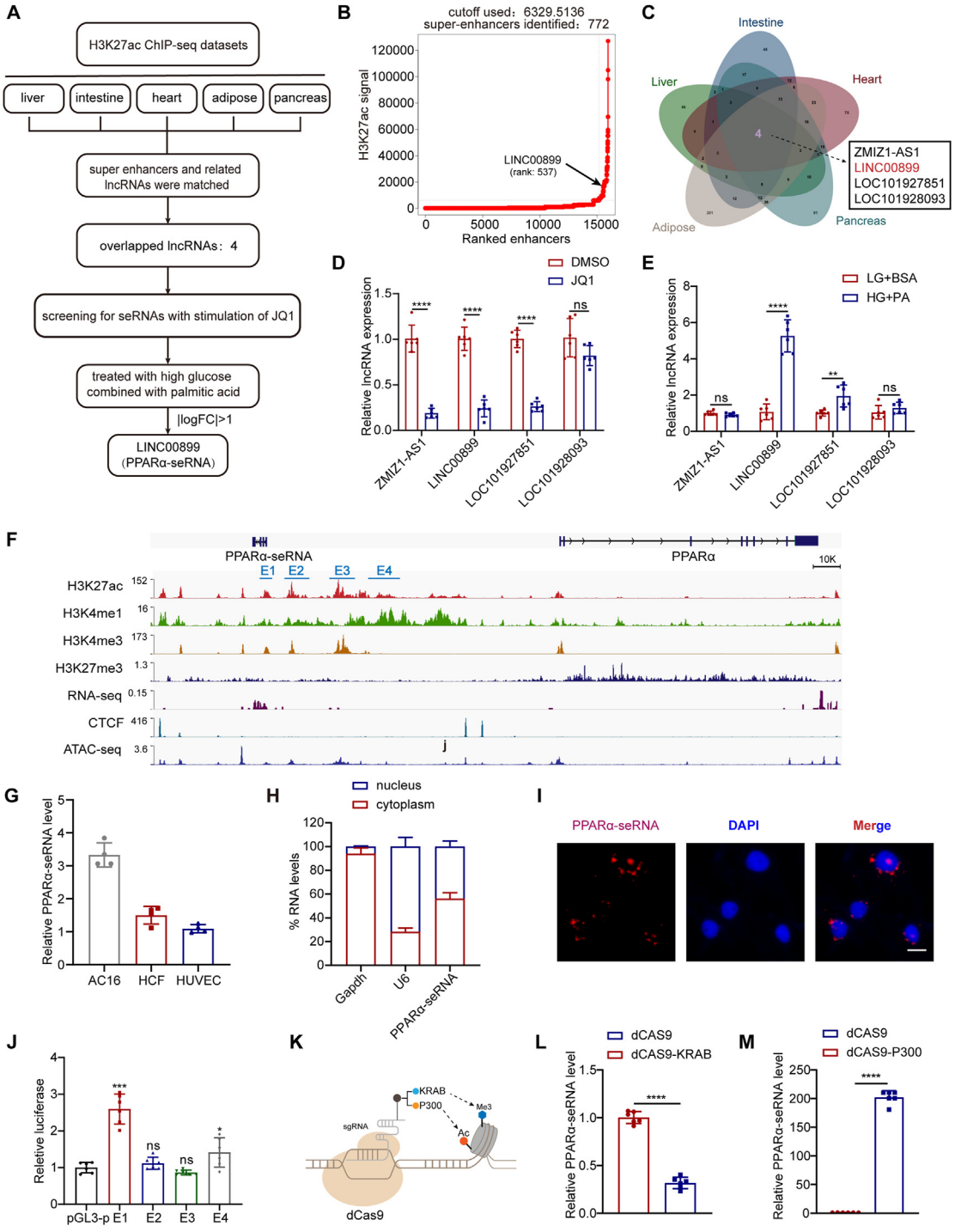

Figure 1: Identification of *PPARα-seRNA* as a key element participating in glucolipid metabolism disorder. (**A**) Selection strategy of DbCM-associated seRNAs from the Encyclopedia of DNA Elements (ENCODE) datasets in different human tissues. **(B)** Rank Ordering of Super-Enhancers (ROSE) algorithm to identify super enhancer and its related gene in heart. **(C)** Identification of potential super-enhancer-related long noncoding RNAs (lncRNAs) expressed in different metabolic tissues and heart by Venn diagram. **(D)** Expression of super-enhancer-related lncRNAs in AC16 treated with the BRD4 inhibitor JQ1 at 1 mmol/L for 24 h. **(E)** Expression of super-enhancer-related lncRNAs according to qRT-PCR in AC16 treated with low (5 mmol/L) or high (33.3 mmol/L) glucose and palmitate (200 μmol/l) for 24 h. (F) ChIP-seq data from WashU website showing peaks of different histone markers. Four constituent enhancers are indicated with short blue lines. **(G)** Relative expression of *PPARα-seRNA* in human cardiomyocyte-like cells (AC16), human cardiac fibroblasts (HCF), and human umbilical vein endothelial cells (HUVECs). (H–I) Subcellular localization of *PPARα-seRNA* detected by qRT-PCR in cytosol and nuclear fractions from AC16 cells (H) and FISH (I, scale bar = 10 μm). *U6* RNA was used as a nucleus RNA marker, while *Gapdh* were used as cytosol RNA marker. **(J)** Activity of four constituent enhancers (E1, E2, E3, and E4) constructed with pGL3-promoter reporter vector, evaluated by luciferase assay. **(K)** Diagram of activated and deactivated enhancer using the CRISPR/dCAS9-p300 or CRISPR/dCAS9-KRAB system with single guide RNA (sgRNA). (L) Expression of *PPARα-seRNA* with super-enhancer deactivated by sgRNA-dCAS9-KRAB. (M) Expression of *PPARα-seRNA* with super-enhancer activated by sgRNA-dCAS9-p300. One-way ANOVA with Tukey's multiple comparisons test was used in (G) and (J); student's two-tailed t test was used otherwise. $^{*}P < 0.05$, $^{**}P < 0.01$, $^{***}P < 0.001$, $^{****}P < 0.0001$, ns, no significant. All data are illustrated as mean ± SD.

luciferase reporters. The results indicated that luciferase activity was the strongest for enhancer 1 (Figure 1J). Notably, we further modulated the histone modification condition of E1 using the CRISPR/dCas9 system. We found that deactivation of E1 inhibited the expression of *PPARα-seRNA*, whereas activation of E1 increased it (Figure 1K-M). Collectively, these results indicated that *PPARα-seRNA* was associated with glucolipid metabolism and regulated by one enhancer.

3.2. *PPARα-seRNA* overexpression aggravated glucolipid metabolism disorder *in vitro*

To investigate the biological effect of *PPARα-seRNA* on glucolipid metabolism, we overexpressed *PPARα-seRNA* in cardiomyocytes (Figure 2A). *PPARα-seRNA* overexpression aggravated the accumulation of lipid droplets and free fatty acids induced by high glucose and palmitic acid in AC16 cells (Figure 2B), but the translated peptide

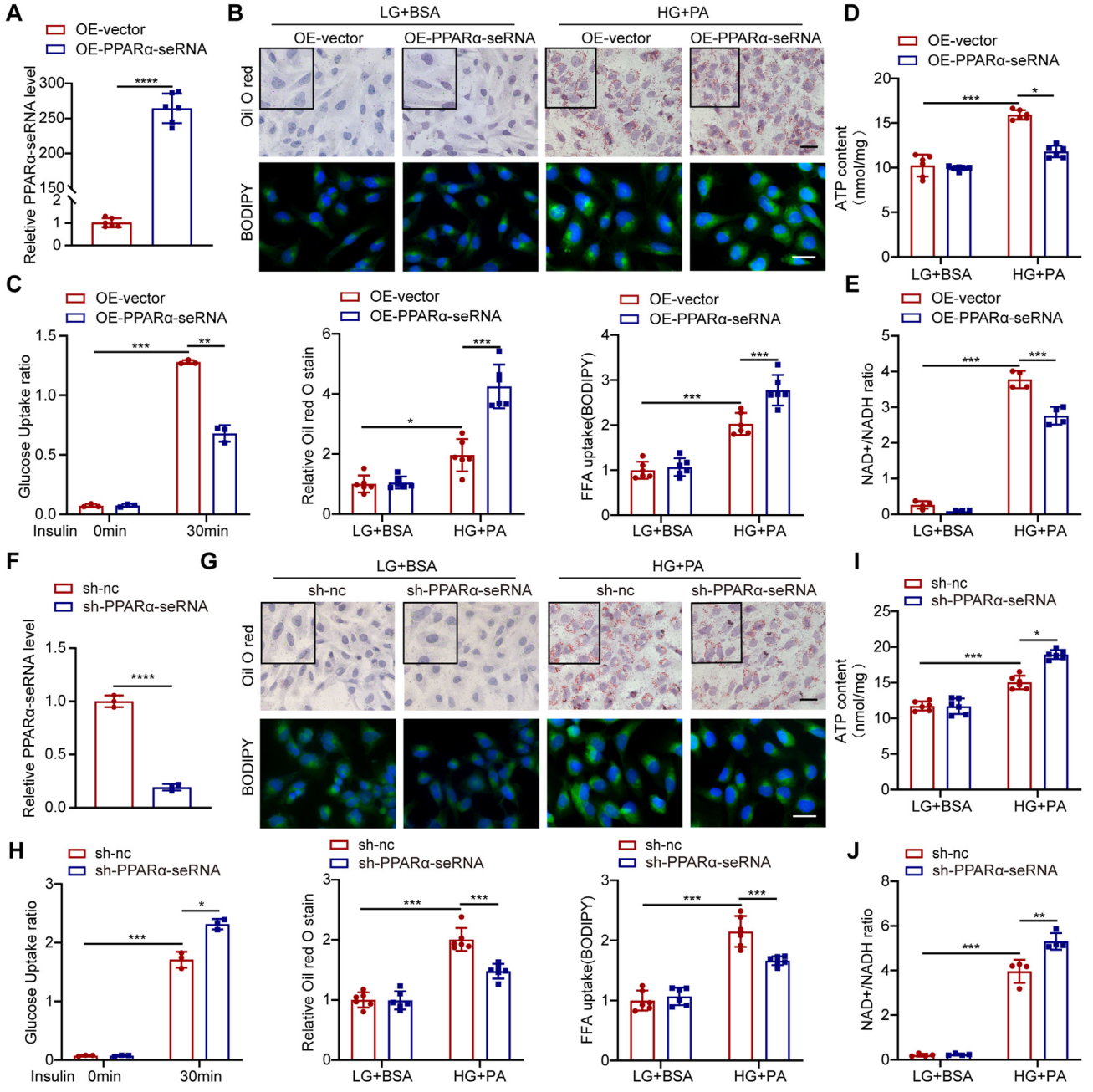

Figure 2: *PPARα-seRNA* aggravates cardiomyocytes metabolic disorders. (A&F) qRT-PCR assay used to detect the effect overexpression (A) and silencing (F) of *PPARα-seRNA* in the AC16 cell line. **(B&G)** Oil O Red (upper panel) and BODIPY staining (lower panel) showing the lipid droplet content after *PPARα-seRNA* overexpression (B) or silencing (G) with high glucose (33.3 mmol/L) for 24 h and palmitate (200 μmol/L) treatment for 6 h. Scale bar = 25 μm. **(C&H)** *In Vitro* Glucose Uptake Assay demonstrating that *PPARα-seRNA* overexpression reduces (C), and *PPARα-seRNA* silencing increases (H) the efficiency of insulin-mediated 2D-glucose uptake. **(D&I)** Total ATP levels declined in response to *PPARα-seRNA* overexpression (D) or decreased when was *PPARα-seRNA* silenced (I) with high glucose (33.3 mmol/L) for 24 h and palmitate (200 μmol/L) treatment for 6 h **(E&J)** *PPARα-seRNA* overexpression reduced (E), and *PPARα-seRNA* silencing increased (J) the NAD+/NADH ratio with high glucose (33.3 mmol/L) for 24 h and palmitate (200 μmol/L) treatment for 6 h. Statistical analysis was performed with student's two-tailed t test in **(A)** and **(F)**. Two-way ANOVA with multiple comparisons tests otherwise. $^{*}P < 0.05$, $^{**}P < 0.01$, $^{***}P < 0.001$, $^{****}P < 0.0001$. Data are depicted as mean ± SD.

had no effect (Figure S4F). In addition, overexpression of *PPARα-seRNA* decreased glucose absorption induced by insulin, total ATP levels, and the ratio of NAD+/NADH in cardiomyocytes (Figure 2C—E & Figure S5A). Conversely, *PPARα-seRNA* silencing reduced lipid deposition and increased glucose absorption, total ATP levels and the NAD^+/NADH ratio in cardiomyocytes (Figure 2F—J & Figure S5B). These results indicated that *PPARα-seRNA* aggravated glucolipid metabolic disorder and energy deficiency disorders *in vitro*.

3.3. *PPARα-seRNA* overexpression exacerbated cardiac dysfunction in db/db mice

We next examined the roles of *PPARα-seRNA* in diabetes-induced cardiac dysfunction using adeno-associated virus 9 (rAAV-9) with a cTnT promoter (Figure 3A). As expected, the expression of *PPARα-seRNA* was increased in the heart of db/db mice injected with rAAV9-*PPARα-seRNA* compared with those injected with rAAV9-vector (Figure 3B). Echocardiographic and hemodynamic data indicated that in db/db mice, overexpression of *PPARα-seRNA* exacerbated cardiac dysfunction compared with the control group injected with a AAV9-vector (Figure 3C—I). Furthermore, the overexpression of *PPARα-seRNA* increased the heart weight/tibial length ratio and myocardium size, and elicited severe fibrosis (Figure 3J-L).

To characterize changes in metabolism in response to *PPARα-seRNA* overexpression *in vivo*, we performed Oil Red O staining, and ATP and NAD^+/NADH measurement in the heart tissue of db/db and db/m mice. The data demonstrated that overexpression of *PPARα-seRNA* robustly increased lipid deposition, reduced ATP levels, and decreased the NAD^+/NADH ratio, in agreement with the *in vitro* results (Figure 3M—O). However, no significant differences were observed in blood glucose level or body weight in response to *PPARα-seRNA* overexpression in the heart (Figure S6A-B). The Intraperitoneal Glucose Tolerance Test (IPGTT) and Insulin Tolerance Test (ITT) also indicated that cardiomyocyte-specific overexpression of *PPARα-seRNA* tended to aggravate glucose tolerance and insulin resistance in db/db mice (Figure S6C-D). There were no obvious differences in blood cholesterol levels between the groups (Figure S6E). Collectively, rAAV9-*PPARα-seRNA* treatment aggravated glucolipid metabolic disorder in cardiac tissue, without any concomitant changes in the systemic metabolism.

3.4. *PPARα-seRNA* promoted the transcription of PPARα *in cis*

Previous studies showed that lncRNA can regulate gene expression through multiple mechanisms, and *cis*-regulation is the most common regulation model [18]. Therefore, we firstly focused on the gene adjacent to *PPARα-seRNA*, PPARα, which has been reported to be highly correlated to diabetic cardiomyopathy through the regulation of fatty acid oxidation and energy metabolism [19,20]. The active E1 enhancer promoted the expression of PPARα, while inactive E1 repressed it (Figure S7). Additionally, RNA-seq data from the GTEX database showed that *PPARα-seRNA* levels had a positive correlation with PPARα in human heart tissue (Figure S2C). Therefore, we speculated that *PPARα-seRNA* may modulate the transcription of PPARα to play a role in diabetic cardiomyopathy. Surprisingly, *PPARα-seRNA* overexpression increased the expression of PPARα, both at the RNA and protein levels (Figure 4A&4C), as well as that of target genes modulated by PPARα (Figure 4G). In contrast, *PPARα-seRNA* silencing reduced the expression of PPARα (Figure 4B&4D). *In vivo*, PPARα was also upregulated by *PPARα-seRNA* overexpression, as evidenced by the result of western blot and immunofluorescence (Figure 4E—F). These data demonstrated that *PPARα-seRNA* facilitated PPARα transcription, both *in vitro* and *in vivo*.

In order to investigate whether PPARα plays a role in the glucolipid metabolic disorder induced by *PPARα-seRNA*, we silenced PPARα in cardiomyocytes overexpressing *PPARα-seRNA* and stimulated them by high glucose and palmitic acid. We found that PPARα silencing reversed the effect of lipids accumulation, as detected by Oil red O and BODIPY staining assays (Figure 4H). Moreover, the reduction in total ATP and NAD^+ content, as well as in the NAD^+/NADH ratio, induced by *PPARα-seRNA* overexpression was also reversed (Figure 4I—J & Figure S5C). Taken together, these rescue assays demonstrated that PPARα mediated the function of *PPARα-seRNA* in glucolipid metabolism.

3.5. *PPARα-seRNA* interacted with KDM4B

To further explore the underlying molecular mechanism by which *PPARα-seRNA* modulates the transcription of PPARα, we performed RNA pulldown assay combined with mass spectrometry analysis, and identified 102 proteins that could potentially bind to *PPARα-seRNA*. Gene Ontology (GO) analysis indicated that these proteins were enriched in the chromatin remodeling pathway, implying that *PPARα-seRNA* was likely involved in regulating chromatin structure (Figure 5A). Among the candidate proteins, RB binding protein 4 (RBBP4) and KDM4B, two critical chromatin-remodeling factors, were selected for further analysis (Figure 5B). As a demethylase, KDM4B is involved in the regulation of gene expression at the post-transcriptional level by catalyzing the demethylation of H3K9me3 [21]. RBBP is a subunit of polycomb repressive complex 2 (PRC2), and is involved in the identification and catalysis of trimethylation at H3K27 [22]. However, RNA pull-down and RIP assays demonstrated that *PPARα-seRNA* has a stronger binding intensity with KDM4B (Figure 5C—D). Therefore, KDM4B was selected for further research. Furthermore, *PPARα-seRNA* and KDM4B were shown to be co-localized by RNA FISH combined with immunofluorescence assay (Figure 5E). In addition, we predicted the KDM4B domains involved in binding to *PPARα-seRNA* using the catRAPID tool, and generated truncated KDM4B mutants based on its secondary structure (Figure 5F—G). Both RNA pull-down assays and RIP demonstrated that *PPARα-seRNA* was conjunct with the all domains of KDM4B (Figure 5H—I).

Similarly, we investigated the interaction between lncPpara and KDM4B, which was predicted to be strong by catRAPID. Interestingly, the regions of lncPpara predicted to bind KDM4B were similar to those in *PPARα-seRNA*, suggesting that both lncppara and *PPARα-seRNA* had similar functional sequences (Figure S8A). The potential interaction between lncPpara and KDM4B was also confirmed by RNA pull-down and RIP assays (Figure S8B-C).

3.6. *PPARα-seRNA* facilitated the accumulation of KDM4B in the nucleus

Next, we attempted to investigate how *PPARα-seRNA* affected the function of KDM4B in cardiomyocytes. Changes in *PPARα-seRNA* did not affect KDM4B protein levels (Figure 6A—B). Interestingly, nucleoplasmic protein separation and immunofluorescence assays showed that KDM4B expression was increased in the nucleus and reduced in the cytoplasm in response to *PPARα-seRNA* overexpression, whereas the exact opposite was observed in response to *PPARα-seRNA* knockdown, suggesting that *PPARα-seRNA* promotes KDM4B entry into the nucleus (Figure 6C—F). To further investigate the mechanism of KDM4B nuclear translocation, Co-IP combined with mass spectrometry was performed to identify potential binding partners for KDM4B. Karyopherin subunit alpha 2 (KPNA2), a key nuclear transport protein, was significantly enriched in the mass spectrometry results (Figure 6G—H). In addition, by Co-IP assay, it was verified that KDM4B bound to KPNA2, and *PPARα-seRNA* enhanced this interaction (Figure 6I). In addition, the interaction

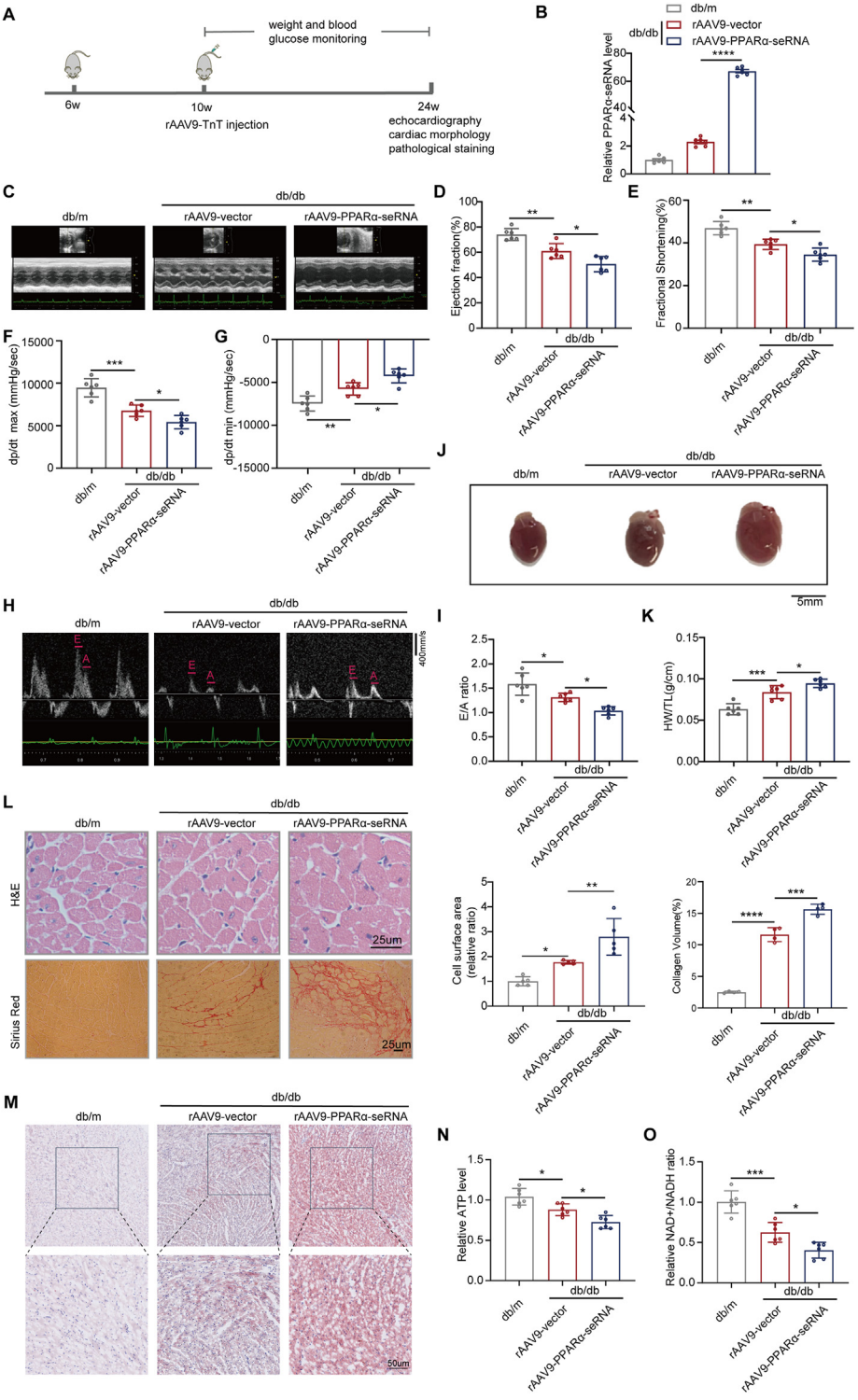

Figure 3: *PPARα-seRNA* overexpression exacerbated cardiac dysfunction in db/db mice. (A) Schematic diagram of the experimental outline using rAAV9-TnT-GFP or rAAV9-TnT-*PPARα-seRNA* injected in db/db mice. **(B)** Expression of *PPARα-seRNA* in heart tissue from db/db and db/m mice. **(C)** Representative M-model of echocardiographic images from treated mice. **(D—E)** Cardiac function presented as ejection fraction (EF) and fractional shortening (FS); n = 6. **(F—G)** Hemodynamic analysis of db/db and db/m mice. dp/dt max, maximal value of the instantaneous first derivative of left ventricular pressure; dp/dt min, minimum peak derivative of pressure over time; n = 6. **(H)** Representative images of pulse-wave Doppler and ratio between mitral E wave and A wave (E/A) in db/db and db/m mice. **(I)** Diastolic function presented as E/A ratio; n = 6. **(J)** Representative images of cardiac general views. **(K)** The ratio of heart weight (HW) to tibial length (TL) in db/db and db/m mice with different treatments; n = 6. **(L)** Representative images of H&E staining (**top**) and sirius red staining (**bottom**) in db/db and db/m mice. Scale bar = 25 μm. **(M)** Representative images of Oil O Red staining in heart from treated mice. Scale bar = 50 μm. **(N—O)** The energy production of diabetic heart assessed by ATP and NAD+/NADH ratio in db/db and db/m mice; n = 6. Statistical analysis was performed with one-way ANOVA with Tukey's multiple comparisons test was used in this part. $*P < 0.05$, $**P < 0.01$, $***P < 0.001$, $****P < 0.0001$. Data are illustrated as mean ± SEM.

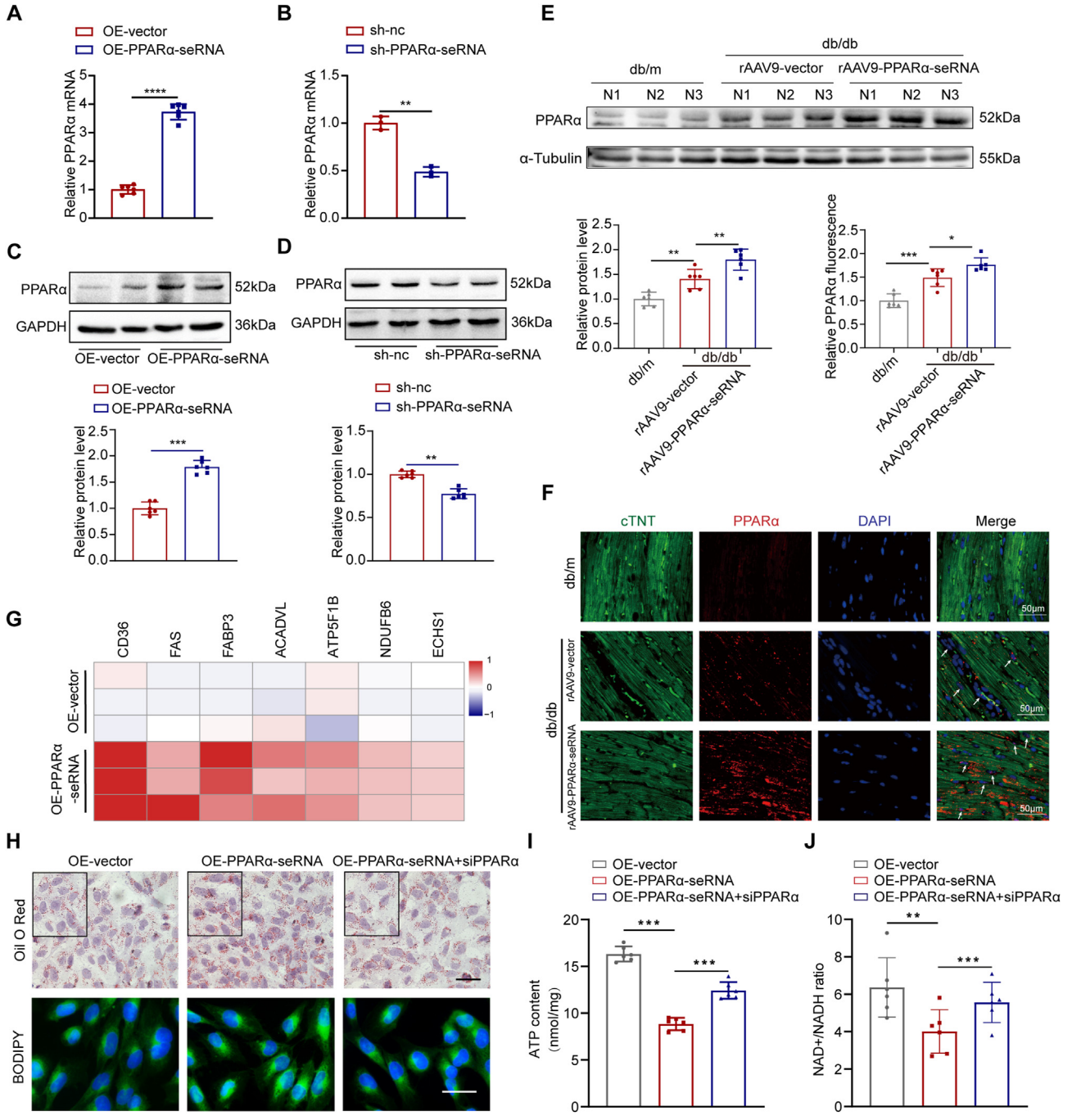

Figure 4: *PPARα-seRNA* promoted the transcription of PPARα *in cis*. **(A-B)** The expression of PPARα by qRT-PCR with *PPARα-seRNA* overexpression or knockdown. **(C-D)** The expression of PPARα by western blot with *PPARα-seRNA* overexpression or knockdown. **(E)** Western blot showing the expression of PPARα in db/db mice with rAAV9- *PPARα-seRNA* treatment. **(F)** Changes of PPARα in cardiac tissue from db/db mice by immunoprecipitation. scale bar = 50 μm. **(G)** Expression of target genes from PPARα signaling pathway determined by qRT-PCR. **(H)** Oil O Red (upper panel) and BODIPY staining (lower panel) showing the lipid droplet content after *PPARα-seRNA* overexpression or PPARα silencing following high glucose (33.3 mmol/L) for 24 h and palmitate (200 μmol/L) treatment for 6 h. Scale bar = 25 μm. **(I-J)** Decreased total ATP levels (I) and NAD+/NADH ratio (J) in response to *PPARα-seRNA* overexpression, ameliorated by PPARα silencing following high glucose (33.3 mmol/L) for 24 h and palmitate (200 μmol/L) treatment for 6 h. Statistical analysis was performed with Student's two-tailed t test for A-D and G; one-way ANOVA with Tukey's multiple comparisons test for E, F, I, and J. $*P < 0.05$, $**P < 0.01$, $***P < 0.001$. Data are illustrated as mean ± SD.

between *PPARα-seRNA* and KPNA2 was confirmed by RNA pulldown and RIP assays (Figure 6J), which indicated that *PPARα-seRNA* maybe serve as a scaffold to connect KDM4B and KPNA2 more closely.

As a histone-modifying enzyme, KDM4B plays an important role in regulating gene expression, which relies on specific histone modifications such as H3K9me3. *PPARα-seRNA* overexpression significantly repressed the level of H3K9me3, whereas PPARα-seRNA silencing promoted it (Figure 6A—B). To explore the role of KDM4B and H3K9me3 in the PPARα promoter, we performed a ChIP assay and found that KDM4B and H3K9me3 were significantly

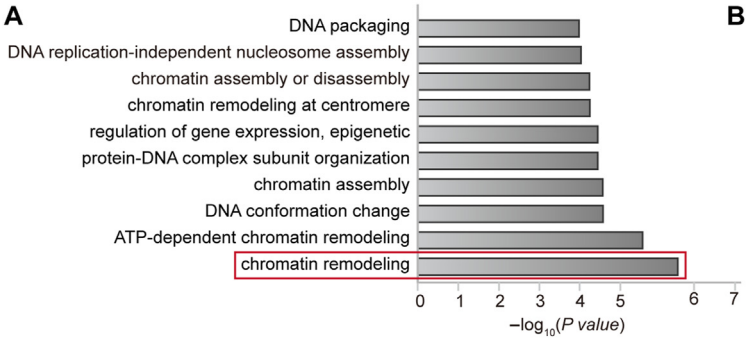

B

proteins participating in chromatin remodeling

Gene	Mw(kDa)	Length	Score	coverage [%]
H3C15	15.388	136	30.09	15.4
H4C1	11.367	103	44.14	40.8
ACTB	41.737	375	97.09	33.3
UBA52	14.728	128	55.53	23.4
HNRNPC	33.67	306	51.54	19.6
NPM1	32.575	294	45.56	20.7
RBBP4	47.656	425	6.98	3.3
NPM3	19.344	178	14.22	9
SMARCA5	121.905	1052	12.98	2.4
KDM4B	121.897	1096	6.32	1.3

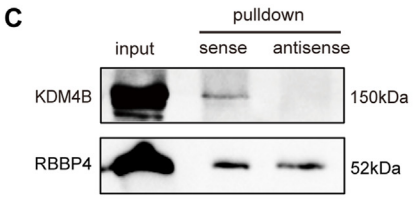

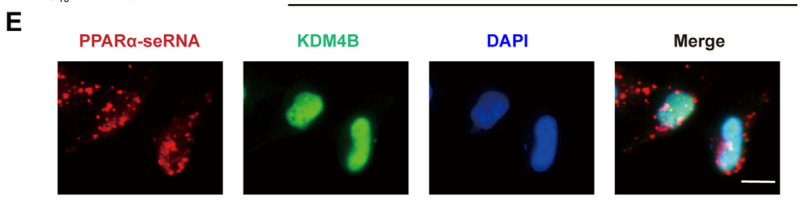

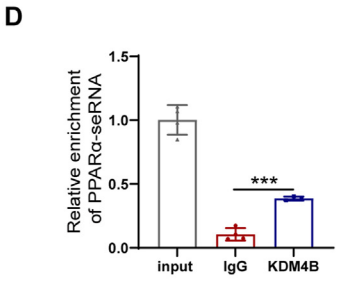

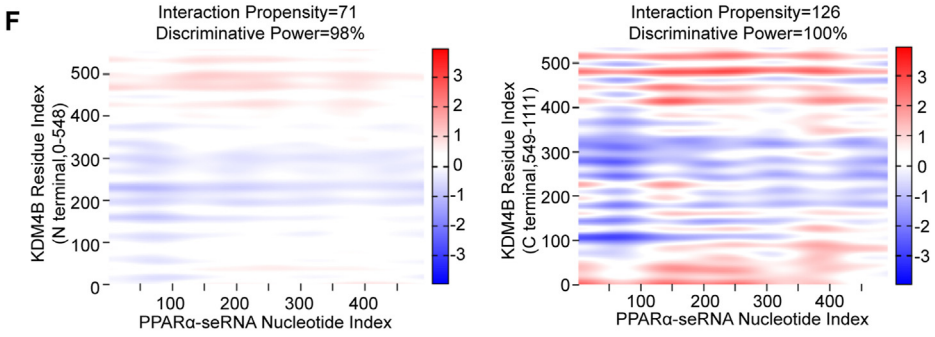

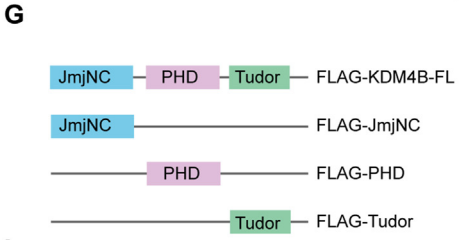

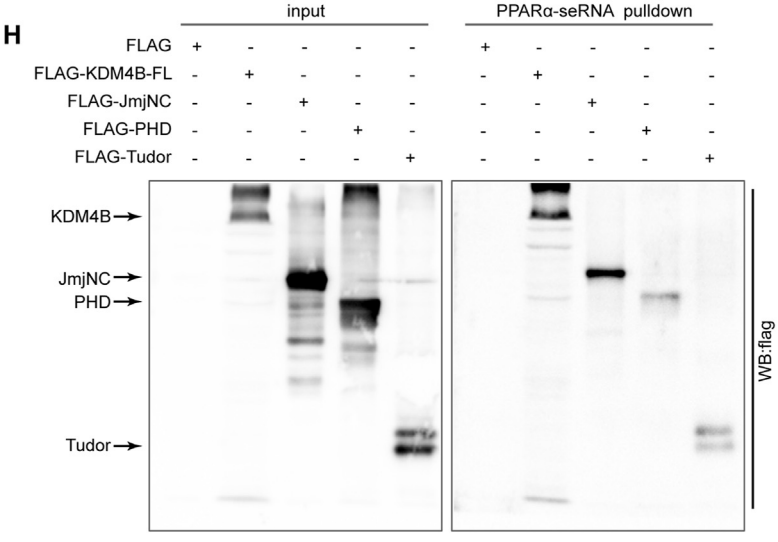

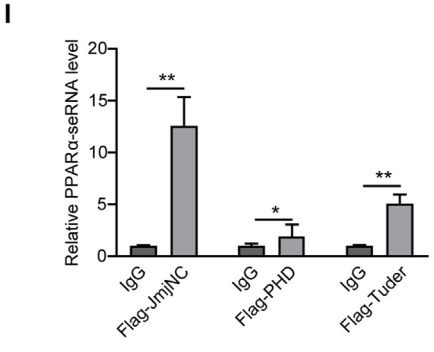

Figure 5: *PPARα-seRNA* interacted with KDM4B. (A) Gene Ontogeny (GO) analysis of *PPARα-seRNA* binding proteins identified by mass spectrometry. **(B)** The detected proteins associated with chromatin remodeling. **(C)** RNA pull-down to detect the binding intensity of KDM4B or RBBP4 with *PPARα-seRNA*. **(D)** RNA immunoprecipitation with an antibody against KDM4B indicating significant enrichment of *PPARα-seRNA*. **(E)** The localization of *PPARα-seRNA* and KDM4B in AC16 cells. Scale bar = 10 μm. **(F)** Binding ability of *PPARα-seRNA* and KDM4B predicted by the catRAPID tool. **(G)** Full length and three domains of KDM4B were inserted into the pc3.1-DNA vector with 3 × flag tag, respectively. **(H)** RNA pull-down verifying the binding intensity of the domains to *PPARα-seRNA*. **(I)** Relative *PPARα-seRNA* levels detected by three domains-RIP in AC16 cells. Statistical analysis was performed with one-way ANOVA with Tukey's multiple comparisons test for D; student's two-tailed t test for I. $^{*}P < 0.05$, $^{**}P < 0.01$. Data are depicted as mean ± SD.

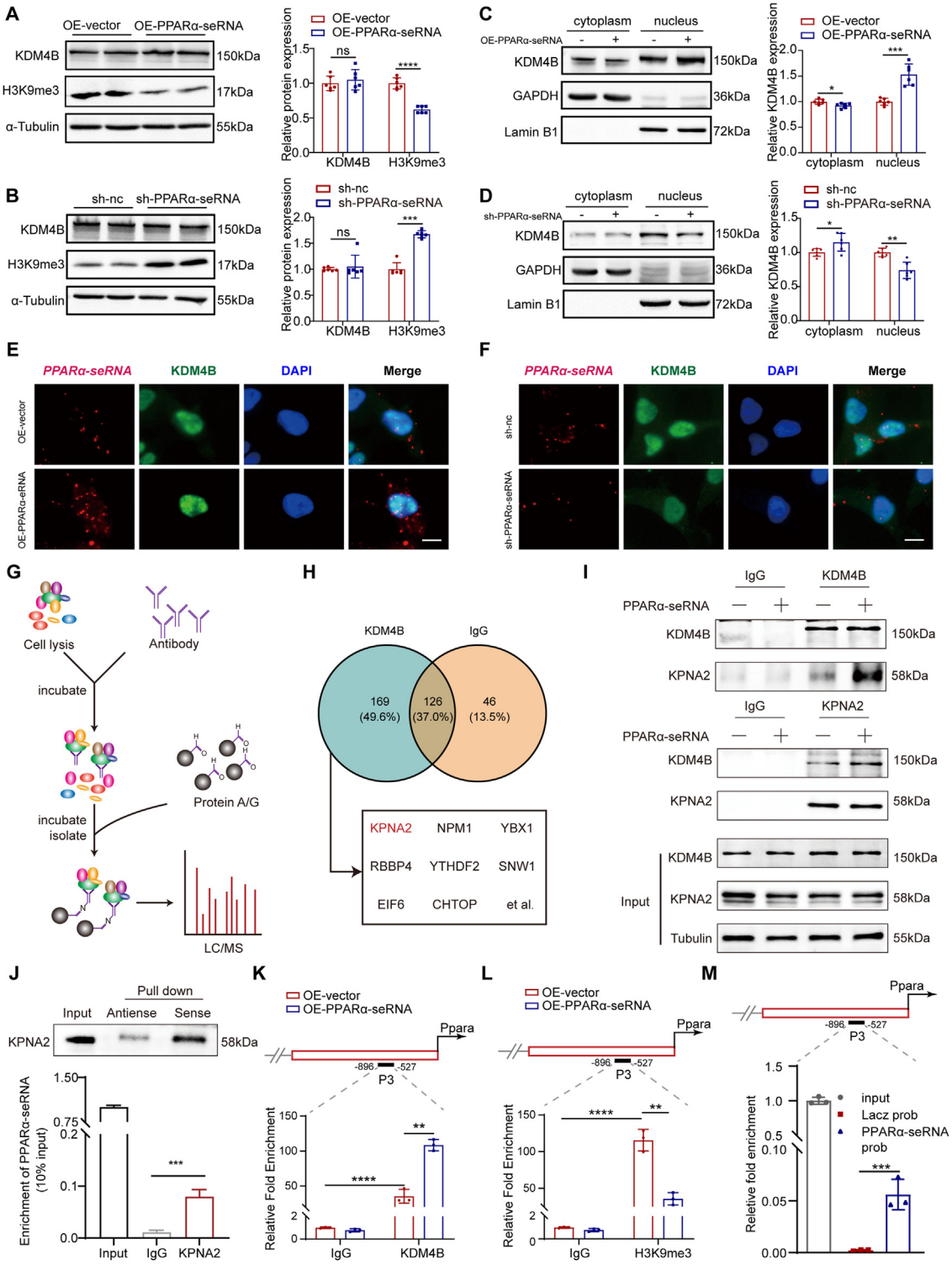

Figure 6: *PPARα-seRNA* facilitated the accumulation of KDM4B in the nucleus. **(A–B)** Western blot showing changes of KDM4B and H3K9me3 after *PPARα-seRNA* overexpression **(A)** or silencing **(B)**. **(C-D)** Western blot showing the subcellular localization of KDM4B after *PPARα-seRNA* overexpression **(C)** or silencing **(D)**. **(E-F)** Immunofluorescence assay showing the expression and subcellular localization of KDM4B after *PPARα-seRNA* overexpression **(E)** or silencing **(F)**. Scale bar = 10 μm. **(G)** Schematic diagram to illustrate the proteins identified by mass spectrometry. **(H)** The proteins enriched by KDM4B identified by mass spectrometry. **(I)** The binding intensity of KDM4B and KPNA2 with or without PPARα-seRNA overexpression detected by Co-IP assay. **(J)** The interaction between PPARα-seRNA and KPNA2 verified by RNA pulldown and RIP assay. **(K-L)** *PPARα-seRNA* overexpression promoted binding of KDM4B and H3K9me3 on the promoter region of PPARα, detected by ChIP-qPCR. **(M)** ChIRP assay performed to verify the binding of *PPARα-seRNA* to the PPARα promoter. One-way ANOVA with Tukey's multiple comparisons test in J and M; student's two-tailed t test for A-D; two-way ANOVA with multiple comparisons test for K and L. $^{*}P < 0.05$, $^{**}P < 0.01$, $^{***}P < 0.001$, $^{****}P < 0.0001$; ns, no significant. Data are depicted as mean ± SD.

enriched in the PPARα promoter, especially in the P3 region. Further, the binding between KDM4B and the PPARα promoter was enhanced by *PPARα-seRNA* overexpression, while the binding intensity of H3K9me3 to the PPARα promoter was decreased (Figure 6K-L). We also performed a ChIRP assay to explore the effect of *PPARα-seRNA* in the PPARα promoter, and observed that *PPARα-seRNA* could bind to the promoter, with P3 being the strongest binding site (Figure 6M). Collectively, these results suggested that *PPARα-seRNA* recruited KDM4B and promoted the accumulation of KDM4B in the nucleus.

3.7. *PPARα-seRNA* promoted glucolipid metabolism disorder via KDM4B

Although the function of KDM4B in lipid metabolism has been studied in adipose tissue, its changes in DbCM have not been characterized. KDM4B was obviously upregulated in response to the stimulation of high glucose and PA in AC16 cells (Figure S9A). In agreement with this, KDM4B protein levels in heart tissue from db/db mice was higher than that in wide-type mice (Figure S9B). Next, we explored the function of KDM4B in cardiac glucolipid metabolism. The results showed that KDM4B silencing resulted in a significant decline in PPARα mRNA and protein levels. In contrast, PPARα expression was enhanced by KDM4B overexpression (Figure 7A—B). In addition, KDM4B overexpression promoted abnormal glucolipid metabolism, while knocking down KDM4B alleviated this disorder (Figure S9C-H).

We wondered whether *PPARα-seRNA*-induced glucolipid metabolism disorder was mediated by KDM4B. To address this question, KDM4B expression was silenced by siRNA transfection into AC16 cells. KDM4B silencing significantly abrogated the increased expression of PPARα promoted by *PPARα-seRNA* overexpression (Figure 7C). KDM4B knockdown reversed the accumulation of lipids induced by *PPARα-seRNA* overexpression (Figure 7D). Similarly, KDM4B silencing prevented the changes in total ATP and NAD^+ content, the NAD^+/NADH ratio, and glucose uptake induced by *PPARα-seRNA* overexpression (Figure 7E—G).

Taken together, these results revealed that KDM4B, as an epigenetic factor, was crucial for the regulation exerted by *PPARα-seRNA* on PPARα expression and glucolipid metabolism in cardiac tissue.

4. DISCUSSION

Metabolic disorder in cardiomyocytes is a critical factor for the progress of diabetic cardiomyopathy. Super enhancer-driven noncoding RNAs have been reported to be novel epigenetic regulators of metabolic changes. In this study, we identified a novel super enhancer-associated ncRNA, *PPARα-seRNA*, which is particularly abundant in cardiomyocytes and is significantly upregulated under pathological conditions of excessive glucose and lipid deposition. Here, *PPARα-seRNA* was shown to promote metabolic disorder and aggravate energy insufficiency in cardiomyocytes. *In vivo*, *PPARα-seRNA* further aggravated cardiac dysfunction associated with glucolipid and energy metabolic disorder. Mechanistically, *PPARα-seRNA* was shown to interact with the histone demethylase KDM4B and promote its translocation to the nucleus, a process mediated by KPNA2. Once in the nucleus, KDM4B repressed the level of H3K9me3 in the PPARα promoter region, and enhanced the transcription of PPARα. This study thus provides a new perspective on the underlying mechanism of diabetic cardiomyopathy.

Super enhancers are active and tissue-specific regulatory elements that enhance core gene transcription [23]. Given that some super-enhancers that exist in multiple tissues may play broader roles in biological processes and have greater value for further research, we focused on super-enhancers and their related molecules in multiple metabolic tissues. Based on H3K27ac ChIP-seq data from four glucolipid metabolic tissues (liver, small intestine, pancreas, and adipose) as well as heart tissue, we identified four super-enhancers and their regulated non-coding RNAs, which could potentially participate in glucolipid metabolism. Eventually, we found that the novel super enhancer-driven non-coding RNA *PPARα-seRNA* has a closer association with glucolipid and energy metabolism in the heart.

In the present study, we employed adeno-associated virus serotype 9 (AAV9) to achieve overexpression of PPARα-seRNA in a murine model of DbCM. The findings indicated a profound exacerbation of cardiac metabolism, whereas there were no significant alterations about the systemic metabolism. This selective metabolic impact is largely attributed to the virus carrying a cardiomyocyte-specific promoter designed to evaluate the effects of PPARα-seRNA on cardiac glucolipid metabolism. To mitigate the influence of other metabolic organs on these outcomes, we also assessed PPARα-seRNA expression in these organs. The results revealed that the overexpression of lncRNA was most obvious in the heart, with comparatively less efficacy in other metabolic tissues. To comprehensively evaluate the physiological roles of PPARα-seRNA, it is preferable to employ transgenic mouse models engineered for systemic knockout.

The function of lncRNAs is dependent on their subcellular localization. LncRNA in the nucleus recruits and combines with transcription factors or regulatory proteins to regulate gene expression at the transcriptional and post-transcriptional levels. In this study, we verified that *PPARα-seRNA* interacted with KDM4B, a key histone demethylase closely related to glucolipid metabolism. Several studies have shown that KDM4B in adipose tissues plays a critical role in lipolysis and energy metabolism by controlling the expression of multiple genes [24]. KDM4B has also been shown to participate in glucose metabolism by regulating the expression of the main glucose transporter GLUT1 via TRAF6-mediated AKT activation [25]. In our study, KDM4B was reduced in the cytoplasm when *PPARα-seRNA* was overexpressed, indicating that *PPARα-seRNA* promotes the nuclear translocation of KDM4B, a necessary requirement for KDM4B to perform its function as a chromatin regulator. Histone modification is an epigenetic regulatory mechanism, and multiple studies have indicated that KDM4B is involved in key cellular events such as the estrogen receptor signaling cascade and mesenchymal cell differentiation via the recruitment and demethylation regulation of repressive H3K9me3 marks at the promoter sequence of target genes [26,27]. Therefore, ChIP-qPCR assay was used to reveal that KDM4B and H3K9me3 were significantly enriched in the PPARα promoter. We also verified the binding of *PPARα-seRNA* to the promoter region of PPARα by ChIRP-qPCR assay, demonstrating that this binding was required to recruit KDM4B.

There are several limitations in the present study. Firstly, lncRNAs are less conserved across species. Although we have identified a murine lncPPARa whose transcript was found to exhibits a sequence identity of 46.5% with *PPARα-seRNA*, we did not further investigate its function on glucolipid metabolic disorders. Secondly, mice with a leptin receptor deficiency (db/m and db/db) were utilized to develop a DbCM mouse model in our study. Transgenic mice in which the myocardium is specifically targeted have not been used yet for further research. In addition, although we verified the interaction between *PPARα-seRNA* and KDM4B, the detailed binding sites were not characterized. In addition, *PPARα-seRNA* was found to localize both in the nucleus and the cytoplasm. In our study, we mainly

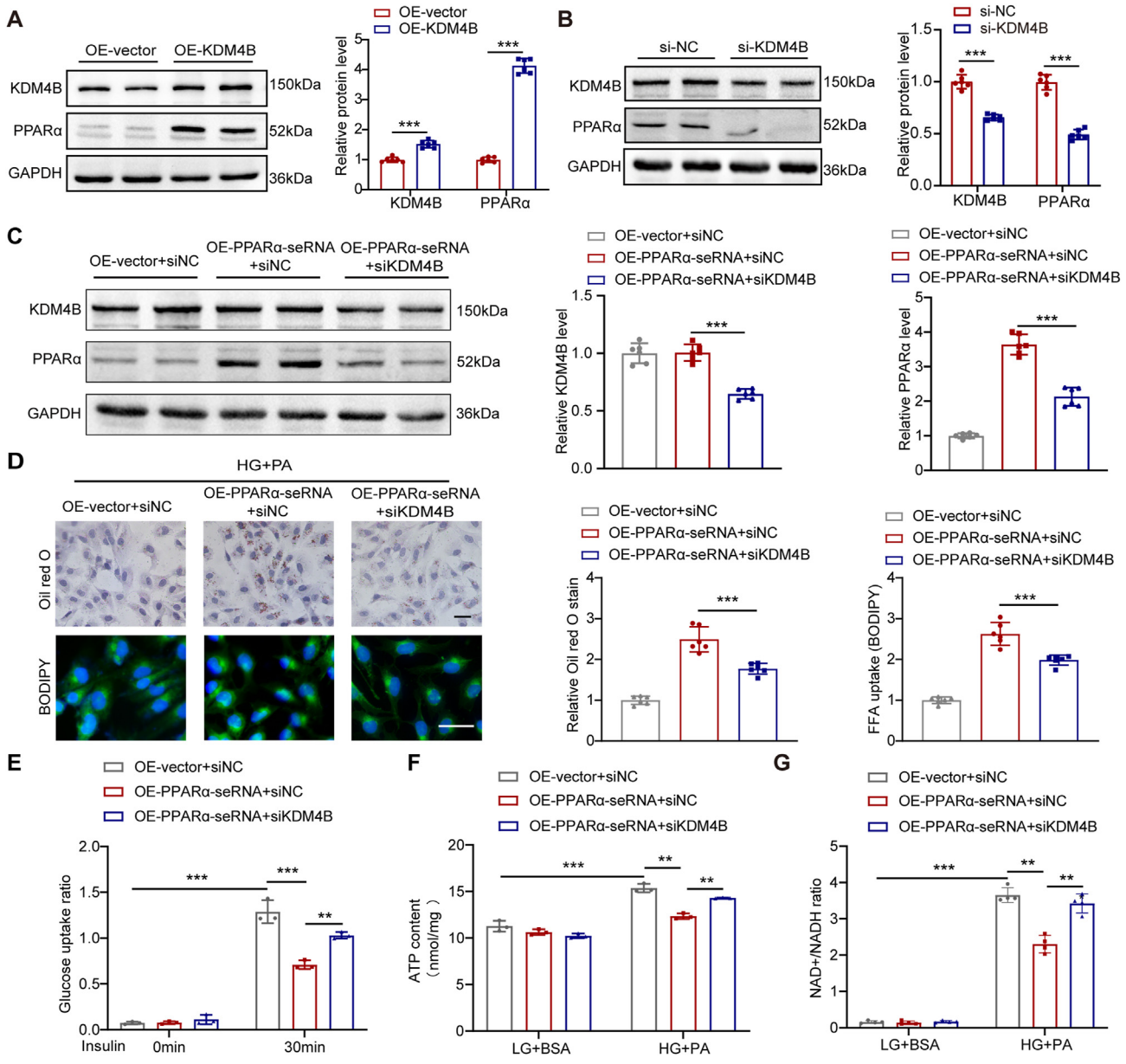

Figure 7: *PPARα-seRNA* promoted glucolipid metabolism disorder via KDM4B. (A–B) Western blot showing the expression of PPARα with KDM4B overexpression **(A)** or reduction **(B)**. **(C)** KDM4B silencing reversed the effect on PPARα induced by *PPARα-seRNA* overexpression. **(D)** Oil O Red (upper panel) and BODIPY staining (lower panel) showing that KDM4B silencing ameliorates lipid droplet accumulation in cardiomyocytes caused by *PPARα-seRNA* overexpression with high glucose (33.3 mmol/L) for 24 h and palmitate (200 μmol/L) treatment for 6 h. Scale bar = 25 μm. **(E-G)** KDM4B silencing improved the capacity for glucose uptake and energy production affected by *PPARα-seRNA* overexpression with high glucose (33.3 mmol/L) for 24 h and palmitate (200 μmol/L) treatment for 6 h. Statistical analysis was performed with student's two-tailed t test for A and B; one-way ANOVA with Tukey's multiple comparisons test in C and D; two-way ANOVA with multiple comparisons test in E-G. $^{*}P < 0.05$, $^{**}P < 0.01$, $^{***}P < 0.001$, $^{****}P < 0.0001$; ns, no significant. Data are depicted as mean ± SD.

focused on its role on the regulation of transcription within the nucleus. Determining what roles it might play in the cytoplasm would require additional experiments. Finally, we could not analyze the expression of *PPARα-seRNA* in cardiac tissue from DbCM patients due to the unavailability of appropriate samples. Further investigation of the mechanisms of action of *PPARα-seRNA* may provide an interesting and novel clinical perspective on diabetic cardiomyopathy. In conclusion, this study suggests that *PPARα-seRNA* is a critical epigenetic regulator of glucolipid and energy metabolism in diabetic cardiomyopathy, and proposes a novel epigenetic mechanism that involves the modulation of histone modifications. *PPARα-seRNA* is therefore a promising target for the treatment of diabetic cardiomyopathy.

FUNDING

This study was supported by grants from Hubei Key Research and Development Program (No. 2021BCA121) and the National Natural Science Foundation of China (Grant numbers: 82170392 and 82170348).

CREDIT AUTHORSHIP CONTRIBUTION STATEMENT

Xiaozhu Ma: Writing — review & editing, Writing — original draft, Methodology, Investigation, Data curation. **Shuai Mei:** Writing — review & editing, Writing — original draft, Methodology, Formal analysis, Data curation. **Qidamugai Wuyun:** Methodology. **Li Zhou:** Methodology. **Ziyang Cai:** Methodology. **Hu Ding:** Writing — review & editing, Validation, Supervision, Funding acquisition. **Jiangtao Yan:** Writing — review & editing, Validation, Supervision, Funding acquisition.

DECLARATION OF COMPETING INTEREST

The authors declare no conflict of interests.

DATA AVAILABILITY

The data that has been used is confidential.

APPENDIX A. SUPPLEMENTARY DATA

Supplementary data to this article can be found online at https://doi.org/10.1016/j.molmet.2024.101978.

REFERENCES

[1] Seferović PM, Paulus WJ. Clinical diabetic cardiomyopathy: a two-faced disease with restrictive and dilated phenotypes. Eur Heart J 2015;36(27):1718—27. 1727a-1727c.

[2] Jia G, Hill MA, Sowers JR. Diabetic cardiomyopathy: an update of mechanisms contributing to this clinical entity. Circ Res 2018;122(4):624—38.

[3] Ke J, Pan J, Lin H, Gu J. Diabetic cardiomyopathy: a brief summary on lipid toxicity. ESC Heart Fail 2023;10(2):776—90.

[4] Tong M, Saito T, Zhai P, Oka SI, Mizushima W, Nakamura M, et al. Mitophagy is essential for maintaining cardiac function during high fat diet-induced diabetic cardiomyopathy. Circ Res 2019;124(9):1360—71.

[5] Zhan J, Chen C, Wang DW, Li H. Hyperglycemic memory in diabetic cardiomyopathy. Front Med 2022;16(1):25—38.

[6] Pott S, Lieb JD. What are super-enhancers? Nat Genet 2015;47(1):8—12.

[7] Feng Y, Xu W, Zhang W, Wang W, Liu T, Zhou X. LncRNA DCRF regulates cardiomyocyte autophagy by targeting miR-551b-5p in diabetic cardiomyopathy. Theranostics 2019;9(15):4558—66.

[8] Han P, Li W, Lin CH, Yang J, Shang C, Nuernberg ST, et al. A long noncoding RNA protects the heart from pathological hypertrophy. Nature 2014;514(7520):102—6.

[9] Li SY, Zhu Y, Li RN, Huang JH, You K, Yuan YF, et al. LncRNA Lnc-APUE is repressed by HNF4α and promotes G1/S phase transition and tumor growth by regulating MiR-20b/E2F1 Axis. Adv Sci 2021;8(7):2003094.

[10] Peng JY, Cai DK, Zeng RL, Zhang CY, Li GC, Chen SF, et al. Upregulation of superenhancer-driven LncRNA FASRL by USF1 promotes de novo fatty acid biosynthesis to exacerbate hepatocellular carcinoma. Adv Sci 2022;10(1):e2204711.

[11] Yuan XQ, Zhou N, Wang JP, Yang XZ, Wang S, Zhang CY, et al. Anchoring super-enhancer-driven oncogenic lncRNAs for anti-tumor therapy in hepatocellular carcinoma. Mol Ther 2023;31(6):1756—74.

[12] Zhang Y, Huang YX, Wang DL, Yang B, Yan HY, Lin LH, et al. LncRNA DSCAM-AS1 interacts with YBX1 to promote cancer progression by forming a positive feedback loop that activates FOXA1 transcription network. Theranostics 2020;10(23):10823—37.

[13] Micheletti R, Plaisance I, Abraham BJ, Sarre A, Ting CC, Alexanian M, et al. The long noncoding RNA Wisper controls cardiac fibrosis and remodeling. Sci Transl Med 2017;9(395).

[14] Wang Z, Zhang XJ, Ji YX, Zhang P, Deng KQ, Gong J, et al. The long noncoding RNA Chaer defines an epigenetic checkpoint in cardiac hypertrophy. Nat Med 2016;22(10):1131—9.

[15] Wang J, Xiang D, Mei S, Jin Y, Sun D, Chen C, et al. The novel long noncoding RNA Lnc19959.2 modulates triglyceride metabolism-associated genes through the interaction with Purb and hnRNPA2B1. Mol Metab 2020;37:100996.

[16] Jia Q, Tan Y, Li Y, Wu Y, Wang J, Tang F. JUN-induced super-enhancer RNA forms R-loop to promote nasopharyngeal carcinoma metastasis. Cell Death Dis 2023;14(7):459.

[17] Herzig S, Shaw RJ. AMPK: guardian of metabolism and mitochondrial homeostasis. Nat Rev Mol Cell Biol 2018;19(2):121—35.

[18] Gil N, Ulitsky I. Regulation of gene expression by cis-acting long non-coding RNAs. Nat Rev Genet 2020;21(2):102—17.

[19] Hu T, Wu Q, Yao Q, Yu J, Jiang K, Wan Y, et al. PRDM16 exerts critical role in myocardial metabolism and energetics in type 2 diabetes induced cardiomyopathy. Metabolism 2023;146:155658.

[20] Yin Z, Zhao Y, He M, Li H, Fan J, Nie X, et al. MiR-30c/PGC-1β protects against diabetic cardiomyopathy via PPARα. Cardiovasc Diabetol 2019;18(1):7.

[21] Sulkowski PL, Oeck S, Dow J, Economos NG, Mirfakhraie L, Liu Y, et al. Oncometabolites suppress DNA repair by disrupting local chromatin signalling. Nature 2020;582(7813):586—91.

[22] Glancy E, Ciferri C, Bracken AP. Structural basis for PRC2 engagement with chromatin. Curr Opin Struct Biol 2021;67:135—44.

[23] Whyte WA, Orlando DA, Hnisz D, Abraham BJ, Lin CY, Kagey MH, et al. Master transcription factors and mediator establish super-enhancers at key cell identity genes. Cell 2013;153(2):307—19.

[24] Cheng Y, Yuan Q, Vergnes L, Rong X, Youn JY, Li J, et al. KDM4B protects against obesity and metabolic dysfunction. Proc Natl Acad Sci U S A 2018;115(24):E5566—75.

[25] Li H, Lan J, Wang G, Guo K, Han C, Li X, et al. KDM4B facilitates colorectal cancer growth and glucose metabolism by stimulating TRAF6-mediated AKT activation. J Exp Clin Cancer Res 2020;39(1):12.

[26] Gaughan L, Stockley J, Coffey K, O'Neill D, Jones DL, Wade M, et al. KDM4B is a master regulator of the estrogen receptor signalling cascade. Nucleic Acids Res 2013;41(14):6892—904.

[27] Ye L, Fan Z, Yu B, Chang J, Al Hezaimi K, Zhou X, et al. Histone demethylases KDM4B and KDM6B promotes osteogenic differentiation of human MSCs. Cell Stem Cell 2012;11(1):50—61.

